Stability analysis of a thinning electrified jet under nonisothermal conditions

Dharmansh Deshawar and Paresh Chokshi ⬤*

Department of Chemical Engineering, Indian Institute of Technology Delhi, New Delhi 110016, India

The linear stability of a jet propagating under an electric field is analyzed under nonisothermal conditions. The electrified jet of a Newtonian fluid is modeled as a slender filament, and the leaky dielectric model is used to account for the Maxwell stresses within the fluid. The convective heat transfer from high-temperature jet to the surroundings results in formation of thicker fibers owing to increased viscosity upon cooling. The jet exhibiting substantial thinning under the action of tangential electric field is examined for stability toward axisymmetric nonperiodic disturbances. This is in contrast to most prior studies which analyzed the stability of a cylindrical jet of uniform radius *without* thinning under extensional flow by examining only *periodic* disturbances. Two case studies of reference fluids differing in viscosity and electrical properties are examined. The spectrum of discrete growth rates for axisymmetric disturbances reveal qualitatively distinct instabilities for the two fluids. For a fluid with high electrical conductivity, the conducting mode driven by the coupling of surface charges and an external electric field is found to be the dominant mode of instability. On the contrary, for low conductivity materials, the surface-tension-driven capillary mode is found to be the most critical mode. Heat transfer from the jet to the surroundings tends to stabilize both types of instability mode. Under sufficiently strong heat transfer, the axisymmetric instability, which is believed to be responsible for producing nanofibers with diametric oscillations in electrospinning process, is suppressed. The stabilization is attributed to the enhancement of viscous stress in the thinning jet upon cooling. It is observed that the stabilization effect is relatively more pronounced in a thinning jet compared to the cylindrical jet of uniform radius. The effects of various material and process parameters on the stability behavior is also examined.

DOI: 10.1103/PhysRevE.103.023107

I. INTRODUCTION

Nanofibers are increasingly gaining attention due to their potential applications in nanofiltration, tissue engineering, medical devices, fuel cell, chemical processes, and targeted drug delivery [1]. The nanosized fibers are produced from electrospinning technique in which the filament is drawn by the application of an external electric field. The tangential electric field acting on the charges present at the fluid-air interface generates a very high elongational strain in the fluid leading to fiber formation [2,3]. The electrified jet traveling under axial electric field often encounters an axisymmetric instability which manifests in the form of sustained oscillations in fiber diameter. In electrospinning process, the nonuniform fibers with thick-thin variations are undesirable. However, the growing axisymmetric instability culminating in to capillary jet break up is essential for electrospraying applications. The comprehensive understanding of the stability behavior of an electrified jet is, therefore, very useful to be able to control the onset of the instability and eventual quality of the final product.

While electrospinning technique is employed for polymeric fluids, there have been several theoretical studies treating the fluid as Newtonian as a limiting case of fluid with low elasticity [4,5]. Hohman *et al.* [4] and Gãñan Calvo [6] developed an electrohydrodynamic formulation using leaky

dielectric model [7] to describe the tangential electric stresses generated by the combined effect of electric field and surface charge density. Using this electrohydrodynamic model, Feng [8,9] proposed a mathematical model to capture the dynamics and axial profiles of jet parameters for both Newtonian and viscoelastic fluids. The stability analysis of an electrified jet under isothermal condition has also been extended to viscoelastic fluids in many recent studies [10–12]. Overall, an electrified jet encounters two qualitatively distinct axisymmetric instability modes, viz. the capillary mode (surface-tension-driven Rayleigh-Plateau instability), and the conducting mode (driven by the destabilizing effect of surface charge and axial electric field). In addition, the electrospinning process exhibits a nonaxisymmetric instability leading to the whipping motion of fiber. While capillary mode is dominant for fluids with low electrical conductivity subjected to weak electric field, for highly conductive fluid under strong electric field, the conducting mode becomes the leading mode [4,13,14]. The axisymmetric instability is believed to be responsible for the formation of undesirable beaded fibers. The instability associated with the electrospraying conditions in the presence of a radial electric field has been analyzed for a perfectly conducting fluid [15,16] and a leaky dielectric fluid [17].

A limited number of studies have also addressed the nonlinear progression of axisymmetric instability of the electrified jets of Newtonian fluid. Lopez-Herrera *et al.* [15] developed a model to investigate the nonlinear deformation and break-up of an electrically charged viscous liquid jet of infinite conductivity. The nonlinear dynamics of a perfectly

_____

*paresh@chemical.iitd.ac.in

conducting jet under radial electric field has been examined for both viscous and viscoelastic liquid [18,19] The analysis predicts the onset of bead formation along the jet. For sufficiently high magnitude of electric field, the beads-on-a-string morphology transitions to structure with spikes [20,21].

In all prior studies, the stability is examined for a cylindrical jet with uniform radius. Not only the thinning of jet radius under electric field but also the variation in axial electric field and surface charge density along the jet have been ignored in the stability analysis of uniform cylinder. Recent studies by Dharmansh and Chokshi [22] (for Newtonian fluid) and Deshawar and Chokshi [23] (for viscoelastic fluid) considered the jet as fiber thinning under realistic electrospinning conditions. The *thinning* jet is found to be relatively more stable compared to the *uniform* jet. The order of magnitude reduction in disturbance growth rate vis-à-vis uniform jet is attributed to taking in to account the deformation rate of the jet as well as axial variation in surface charge density and electric field within the jet. The stability of a thinning polymeric fiber in a mechanical drawing process has also been examined in a series of linear as well as weakly nonlinear stability analyses [24–27].

While stability behavior of thinning jet in the absence of heat transfer and mass transfer (solvent evaporation) from the fluid to the surrounding air is well-studied, the stability analysis examining role of convective heat transfer and solvent evaporation in growth of axisymmetric disturbance has not gained sufficient attention. The nonisothermal condition is mostly relevant for electrospinning of polymeric melt. Following the earlier experimental study by Larrondo and Manley [28] demonstrating the potential of melt electrospinning, there have been a number of theoretical and experimental studies of high-temperature electrospinning [1,29–35]. Melt electrospinning is best suited under circumstances in which solvent removal and recovery need to be eliminated to render the process environmentally and economically favorable. Recently, the role of solvent evaporation in instability of an electrified jet of polymeric solution under isothermal condition is studied by Deshawar *et al.* [36]. Separate viscoelastic models for unentangled and entangled polymeric solution were adopted for rheological description of the fluid. The rheological modification upon solvent removal is found to suppress the axisymmetric instability producing smooth nanofibers.

In present study, the axisymmetric instability in a Newtonian jet is analyzed under nonisothermal condition resulting due to convective heat transfer from the jet to the surrounding air. The spectrum of disturbance growth rates is constructed for nonperiodic axisymmetric disturbances imposed on a *thinning* jet under the action of an axial electric field. The modification of fluid properties, importantly viscosity upon cooling is believed to play an important role in controlling the onset of instability leading to diametric oscillations along the jet. The reference parameters are selected to represent realistic electrospinning conditions for two different fluids—one with high electrical conductivity and low viscosity and the other with low electrical conductivity and high viscosity. Similar systems have been previously examined for linear stability under isothermal conditions by Dharmansh and Chokshi [22]. The present work extends this study to incorporate the heat transfer phenomenon.
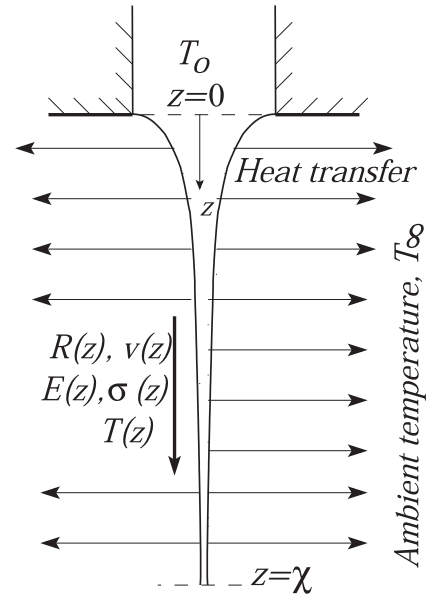

FIG. 1. Schematic of nonisothermal electrospinning process.

II. PROBLEM FORMULATION

A. Mathematical model of an electrified jet

The process of electrospinning comprises of a nozzle with fluid and a collector plate across which a potential difference is applied. The imposed electric field drives fluid which emanates from the nozzle in the form of a filament which traverses toward the bottom collector plate as shown in Fig. 1. The plate and the nozzle are maintained at opposite polarities of the electric field to maintain the flow. As jet emerges, it initially travels in a straight linear path and experiences significant thinning due to the tangential electric stress resulting from the surfaces charges under the action of electric field. After some distance from the nozzle, the jet undergoes whipping motion due to the bending instability. Finally, the fiber is deposited on the collector plate. The emphasis of the present study is restricted to the linear straight jet part of the motion. The straight jet is modeled as one-dimensional slender-body filament such that radial variations of the jet variables, like velocity, electric field and temperature, are ignored and only axial variations are considered. Under nonisothermal conditions, the jet exchanges thermal energy with the environment by convective heat transfer. Since the focus is on analyzing axisymmetric instability during the straight jet motion responsible for diametric oscillations, the whipping motion is not considered. Moreover, the solvent evaporation which is more prominent during the whipping motion is considered negligible during the short distance of linear motion. This allows the present analysis to be equally valid for both molten material or solutions. The weakly elastic molten polymer with very short relaxation time can be modeled as a Newtonian fluid.

The cooling of the high-temperature jet as a result of heat transfer to the surrounding affects the temperature sensitive properties. Most importantly, the viscosity variation along the jet plays an important role in jet dynamics as well as its stability behavior. The surface tension and density of the fluid are assumed unaffected by the extent of temperature change in

jet from nozzle to the collector plate. The mathematical model of jet dynamics is similar to the one employed in the earlier studies of isothermal jet [8,22]. A leaky dielectric model given by Melcher and Taylor [7] and Saville [37] is used to describe the characteristics of the conductive fluid under an external electric field. The jet variables are radius R, velocity v, surface change density σ, temperature T and axial electric field within the jet E. The governing equations of jet dynamics are

$$\frac{\partial R^2}{\partial t} + \frac{\partial (R^2 v)}{\partial z} = 0, \tag{1}$$

$$\rho \left(\frac{\partial v}{\partial t} + v \frac{\partial v}{\partial z} \right)$$

$$= \rho g + \frac{1}{\pi R^2} \frac{\partial}{\partial z} \left[\pi R^2 \frac{\partial}{\partial z} \left(3\eta \frac{\partial v}{\partial z} \right) \right] + \frac{\gamma}{R^2} \frac{\partial R}{\partial z}$$

$$+ \frac{\sigma}{\epsilon_0} \frac{\partial \sigma}{\partial z} + (\epsilon - \epsilon_0) E \frac{\partial E}{\partial z} + \frac{2\sigma E}{R}, \tag{2}$$

$$\frac{\partial (2\pi R \sigma)}{\partial t} + \frac{\partial}{\partial z} (\pi R^2 K E + 2\pi R v \sigma) = 0, \tag{3}$$

$$\epsilon_0 (E_\infty - E) = \ln \left(\frac{L}{R_0} \right) \left[\frac{\partial}{\partial z} (\sigma R) - \frac{\epsilon - \epsilon_0}{2} \frac{\partial^2}{\partial z^2} (E R^2) \right], \tag{4}$$

$$\rho C_p \left(\frac{\partial T}{\partial t} + v \frac{\partial T}{\partial z} \right) = -\frac{2h(T - T_\infty)}{R} + 3\eta \left(\frac{\partial v}{\partial z} \right)^2. \tag{5}$$

Here, Eqs. (1)–(5) are the conservation of mass, momentum, charge, electric field, and thermal energy, respectively. R_0 and v_0 are the jet radius and velocity, respectively, at the tip of the nozzle and Q represents the fluid flow rate through the nozzle. ρ, η, and γ are the local density, viscosity, and surface tension of the fluid, respectively. The momentum conservation represents the balance of the gravitational, surface tension, viscous, inertial, and electric forces generated by the Maxwell stresses using the jump conditions described by Dharmansh and Chokshi [22]. In the charge conservation Eq. (3), K is the electrical conductivity and I denote the electric current passing through the jet. The surface charge density σ accounts for both free and induced charges. Since electrical conductivity is generally not very high in nonisothermal spinning, K is assumed to be temperature independent. The governing equation for the electric field, Eq. (4), is nicely derived in Hohman *et al.* [4] by assuming the charges within the jet as localized along the jet axis with an effective linear charge density which is obtained using the Gauss' law. The electrostatic potential is then estimated with the help of Coulomb's law which, in turn, provides the slender-filament approximation for the axial electric field. The equation estimates the distortion in axial electric field within the jet with respect to the uniform applied potential difference between the electrodes. The thermal energy conservation Eq. (5) takes in to account the change in thermal energy due to convective heat transfer to the surrounding and viscous dissipation within the jet. Here, C_p is the fluid heat capacity, h is the heat transfer coefficient, and T_∞ denotes the constant ambient temperature [27].

The temperature-dependent local viscosity is given by the Arrhenius law,

$$\eta(T) = \eta(T_0) \exp \left[\frac{E_a}{R_{ig}} \left(\frac{1}{T} - \frac{1}{T_0} \right) \right] = \eta(T_0) f(T). \tag{6}$$

Here, E_a is the activation energy, R_{ig} is the ideal gas constant, and $\eta(T_0)$ is the fluid viscosity at the nozzle temperature T_0. This temperature dependence of viscosity is in accordance with the kinetic theory [38], where the viscous force of liquids is associated with overcoming of potential energy barrier given by the activation energy. The heat transfer coefficient is considered a function of the local radius and velocity of the jet [39],

$$h(z) = 0.388 k_{\text{air}} \left(\frac{v}{\nu_{\text{air}} \pi R^2} \right)^{\frac{1}{3}} \left[1 + \left(\frac{8 V_{\text{air}}}{v} \right)^2 \right]^{\frac{1}{6}}, \tag{7}$$

where $h(z)$ is the heat transfer coefficient, which depends on the axial position z. R, and v are the local radius and velocity of the jet, respectively. Further, V_{air} is the air velocity, and k_{air} and ν_{air} are the thermal conductivity and kinematic viscosity of the ambient cooling air, respectively. Thus, heat transfer coefficient is proportional to the speed of surrounding air.

Next, the governing Eqs. (1)–(5) are made dimensionless according to the following rules:

$$R^* \to \frac{R}{R_0}, \quad v^* \to \frac{v}{v_0}, \quad E^* \to \frac{E}{E_0},$$

$$\sigma^* \to \frac{\sigma}{\sigma_0}, \quad T^* \to \frac{T}{T_0}, \quad E_a = \frac{E_a^*}{R_{ig} T_0}, \tag{8}$$

where $v_0 = Q/(\pi R_0^2)$, $E_0 = I/(\pi R_0^2 K)$, and $\sigma_0 = \bar{\epsilon} E_0$. In what follows, the superscript * denoting dimensionless variables is omitted for brevity. The dimensionless governing equations are expressed as

$$\frac{\partial R^2}{\partial t} + \frac{\partial (R^2 v)}{\partial z} = 0, \tag{9}$$

$$\text{Re} \left(\frac{\partial v}{\partial t} + v \frac{\partial v}{\partial z} \right) = \text{Bo} + \frac{1}{\text{Ca}\, R^2} \frac{\partial R}{\partial z} + \frac{\partial}{\partial z} \left[e^{E_a \left(\frac{1}{T} - 1 \right)} \frac{\partial v}{\partial z} \right]$$

$$+ E_f \left(\sigma \frac{\partial \sigma}{\partial z} + \beta E \frac{\partial E}{\partial z} + \frac{2\sigma E}{R} \right), \tag{10}$$

$$\frac{\partial}{\partial t} (R\sigma) + \frac{\partial}{\partial z} (E R^2 + \text{Pe}\, R v \sigma) = 0, \tag{11}$$

$$E = E_\infty - \ln \chi \left[\frac{\partial}{\partial z} (R\sigma) - \frac{\beta}{2} \frac{\partial^2}{\partial z^2} (E R^2) \right], \tag{12}$$

$$\text{Pe}^T \left(\frac{\partial T}{\partial t} + v \frac{\partial T}{\partial z} \right) = \text{Na}\, e^{E_a \left(\frac{1}{T} - 1 \right)} \left(\frac{\partial v}{\partial z} \right)^2 - 2\,\text{Bi}_z \frac{T - T_\infty}{R}. \tag{13}$$

The dimensionless governing Eqs. (9)–(13) feature several dimensionless numbers as summarized in Table I. As case studies, two sets of dimensionless parameters corresponding to two different fluids are considered. Set I represents low viscous solution with very high electrical conductivity [22] and Set II represents weakly elastic molten polymeric fluid with low electrical conductivity and high viscosity [31,35]. The strength of heat transfer is given by the Biot number Bi, a dimensionless hear transfer coefficient. Note that the heat transfer coefficient, and hence the Biot number, depends upon the jet velocity and radius. The local Biot number obtained

TABLE I. List of dimensionless numbers.

Parameter	Dimensionless number	Definition	Set I	Set II
Bo	Bond number	$\frac{\rho g R_0^2}{\eta_0 v_0}$	0.5	10^{-4}
Bi	Biot number	$\frac{h_0 R_0}{k}$	5×10^{-2}	5×10^{-2}
Ca	Capillary number	$\frac{\eta_0 v_0}{\gamma}$	1	4
E_∞	Imposed potential difference	$\frac{\Delta V/L}{E_0}$	250	0.1
E_f	Current strength	$\frac{\bar{\varepsilon} E_0^2}{\rho v_0^2}$	5×10^{-7}	4
Na	Nahme-Griffith number	$\frac{v_0^2 \eta_0}{k T_0}$	5×10^{-5}	5×10^{-4}
Pe	Electric Péclet number	$\frac{2 \bar{\varepsilon} v_0}{K R_0}$	10^{-6}	2
Pe^T	Thermal Péclet number	$\frac{\rho C_P R_0 v_0}{k}$	25	20
Re	Reynolds number	$\frac{R_0 v_0 \rho}{\eta_0}$	5×10^{-3}	2.5×10^{-4}
β	Relative permittivity	$\frac{\epsilon}{\bar{\epsilon}} - 1$	50	2.1
χ	Jet aspect ratio	$\frac{L}{R_0}$	200	200

from Eq. (14) is given as follows:

$$\text{Bi}_z = \text{Bi}\left(\frac{v}{R^2}\right)^{\frac{1}{3}} \left[1 + \left(\frac{8 V_{\text{air}}}{v}\right)^2\right]^{\frac{1}{6}}. \tag{14}$$

Here, $\text{Bi} = h_0 R_0 / k$ represents the Biot number at the nozzle condition and $\text{Bi}_z = h R_0 / k$ represents the dimensionless *local* heat transfer coefficient, $h(z)$, at any point along the jet. The air velocity V_{air} is made nondimensional by v_0. The Nahme-Griffith number Na is a measure of the viscous dissipation. The Bond number Bo is the ratio of the gravitational force to the viscous force. The capillary number Ca represents the ratio of the viscous force and the surface tensor force acting across the fluid-air interface. Pe is the electric Péclet number representing dimensionless electrical conductivity of the fluid. Pe^T is the thermal Péclet number, which is the ratio of the advective and diffusive transport rates for thermal energy. The other nondimensional groups are E_∞, E_f, β, and χ, which represent the imposed potential difference, current strength, relative permittivity, and jet aspect ratio, respectively.

The above governing equations are supported by following boundary conditions:

$$\text{At nozzle:} \ z = 0, \quad R = 1, \quad T = 1, \tag{15}$$

$$\text{At jet end:} \ z = \chi, \quad E(\chi) = E_\infty. \tag{16}$$

The fitting method of Feng [8,9] is employed to estimate E at the nozzle ($z = 0$) from the evaluated surface charge density profile. It is important to note that the initial surface charge density strongly depends upon the geometry of the nozzle and is estimated from the three-dimensional electrostatics around the solid-liquid-air interface which is beyond the scope of the present one-dimensional slender-filament model. In the absence of rigorous calculation of surface charge density in the vicinity of nozzle, an *ad hoc* treatment of estimating the initial charge density based on the slope of the surface charge density profile, $\sigma(z)$, as suggested by Feng [8,9], is adopted. It was shown that estimating the initial surface charge density

by a fitting method will not dramatically alter the jet profile, except for a very short distance away from the nozzle.

The boundary condition for the jet radius at the lower end ($z = \chi$) is not straightforward. For the thinning jet, an asymptotic boundary condition is assumed of the form $R \propto z^{-a}$. The thinning exponent a is obtained by satisfying the balance of the dominant forces in momentum conservation Eq. (10) in the thinned jet at the lower end. The balance of dominant forces and hence evaluation of a are carried out separately for the two sets of fluid parameters summarized in Table I. The first case (Set I) considers fluid with low viscosity and high electrical conductivity. Thus for this fluid, the inertial force dominates over the viscous force and it balances with the electric force (high Re, low Pe). The balance between two dominant forces, inertia and electric, is depicted in next section [Fig. 2(a)]. Here, gravity and surface tension forces are negligible compared to the electrical force generated by coupling of the surface tension and external electric field. Thus, satisfying the balance of inertial and electric forces in the momentum balance equation gives

$$v \frac{dv}{dz} \cong E_f \left(\frac{2 E \sigma}{R}\right). \tag{17}$$

The above balance yields the value of $a = 1/4$. The asymptotic boundary condition at the end of the straight jet ($z = \chi$) thus becomes [8,40]

$$R + 4 z \frac{dR}{dz} = 0. \tag{18}$$

The second case (Set II) considers a highly viscous fluid having low electrical conductivity (low Re, high Pe). In this case, the viscous and electric forces are dominant over the other terms in the momentum balance, as to be discussed in the next section [Fig. 2(b)]. To calculate the exponent a in the asymptotic relation $R \propto z^{-a}$, the following balance holds at the end point:

$$\frac{d}{dz}\left[e^{E_a\left(\frac{1}{T}-1\right)} \frac{dv}{dz}\right] \cong E_f \left(\frac{2 E \sigma}{R}\right). \tag{19}$$

This relation gives the value of $a = -1$. The asymptotic boundary condition at the end of the straight jet ($z = \chi$) thus becomes

$$R + z \frac{dR}{dz} = 0. \tag{20}$$

The steady-state solution of the governing equations is obtained by the ordinary differential equation solver package in COMSOL Multiphysics 4.4 using the finite element numerical scheme.

B. Linear stability analysis

The linear stability analysis is generally carried out by imposing infinitesimally small amplitude disturbances on a *base-state* profile of the jet followed by linearizing the governing equations to the linear order of disturbance amplitude and estimating the growth/decay rate of these axisymmetric
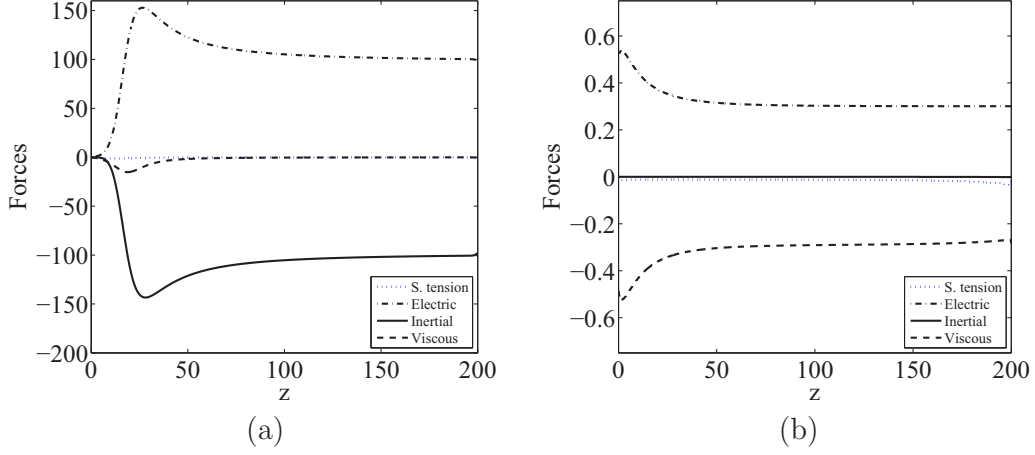
FIG. 2. Magnitude of various dimensionless forces acting on the jet along z direction. (a) Set I: Inertial and electric forces are dominant toward the end of the jet; (b) Set II: Viscous and electric forces are dominant.

disturbances. In most previous studies, the *base-state* profile is often assumed a cylindrical jet of uniform radius with uniform distribution of surface charges and electric field. This simplification ignores the fact that the electrified straight jet stretches and thins during flow because of the applied tangential electric force. Thus, the analysis of a uniform jet fails to take in to account the deformation rate of the jet as well as nonuniform distribution of surface charges and electric field along the jet. In contrast to most prior studies, the present analysis considers as base-state the *thinning jet* profile obtained steady-state solution of the governing equations of jet dynamics. Similar stability analysis of a thinning jet of Newtonian and polymeric fluids under isothermal conditions have been carried out in recent studies [22,23]. The generic jet variable is expanded as superposition of the steady-state (referred to as

base-state) profile and nonperiodic axisymmetric disturbances of infinitesimally small amplitude, as follows:

$$\phi(z,t) = \bar{\phi}(z) + \epsilon\, \tilde{\phi}(z)\, e^{\omega t}, \tag{21}$$

where a generic variable ϕ represents the jet variables R, v, E, σ, and T. $\bar{\phi}(z)$ denotes the steady-state profiles, $\bar{R}(z), \bar{v}(z), \bar{E}(z), \bar{\sigma}(z)$ and $\bar{T}(z)$. $\tilde{\phi}(z)$ represents the disturbance profile, where ϵ denotes the order of amplitude of the imposed disturbance. ω is the complex-valued linear growth rate of the disturbance given by $\omega = \omega_r + i\omega_i$. Here, the real part ω_r is the growth/decay rate and the imaginary-part ω_i represents the disturbance frequency. The disturbance governing equations linearized to $O(\epsilon)$ are of the form

$$2\bar{R}'\bar{v}\tilde{R} + 2\bar{R}\bar{v}'\tilde{R} + 2\bar{R}\bar{R}'\tilde{v} + 2\bar{R}\bar{v}\tilde{R}' + \bar{R}^2\tilde{v}' = -2\,\omega\bar{R}\tilde{R}, \tag{22}$$

$$\mathrm{Re}(\bar{v}'\tilde{v} - \bar{v}\tilde{v}') + \frac{6\exp[E_a(1/\bar{T} - 1)]}{\bar{R}}\left[-\frac{\bar{v}'\bar{R}'\tilde{R}}{\bar{R}} + \bar{v}'\tilde{R}' + \bar{R}'\tilde{v}' + \frac{\bar{R}\tilde{v}''}{2} - \frac{E_a\bar{R}'\bar{v}'\tilde{T}}{\bar{T}^2} \right.$$
$$+ \frac{E_a\tilde{T}\bar{T}'\bar{v}'}{\bar{T}^3}\left(\frac{E_a}{2\bar{T}} + 1\right) - \frac{E_a}{2\bar{T}^2}(\bar{v}'\tilde{T}' + \bar{T}'\tilde{v}' + \tilde{T}\bar{v}'') \left] + \frac{1}{\mathrm{Ca}}\left(\frac{-2\bar{R}'\tilde{R}}{\bar{R}^3} + \frac{\tilde{R}'}{\bar{R}^2} + \tilde{R}''' \right)\right.$$
$$+ E_f\left[\beta(\bar{E}'\tilde{E} + \bar{E}\tilde{E}') + \bar{\sigma}\tilde{\sigma}' + \bar{\sigma}'\tilde{\sigma} + \frac{2}{\bar{R}}\left(\bar{\sigma}\tilde{E} - \frac{\bar{E}\bar{\sigma}\tilde{R}}{\bar{R}} + \bar{E}\tilde{\sigma} \right) \right] = \omega\tilde{v}, \tag{23}$$

$$\tilde{E} - \ln\chi\left[\bar{\sigma}'\tilde{R} + \bar{R}'\tilde{\sigma} + \bar{\sigma}\tilde{R}' + \bar{R}\tilde{\sigma}' - \beta\left(\bar{R}'^2\tilde{E} + \bar{R}\bar{R}''\tilde{E} + \bar{E}''\bar{R}\tilde{R} + 2\bar{E}'\bar{R}'\tilde{R} \right.\right.$$
$$\left.\left. + \bar{E}\bar{R}''\tilde{R} + 2\bar{R}\bar{R}'\tilde{E}' + 2\bar{E}'\bar{R}\tilde{R}' + 2\bar{E}\bar{R}'\tilde{R}' + \frac{\bar{R}^2\tilde{E}''}{2} + \bar{E}\bar{R}\tilde{R}'' \right) \right] = 0, \tag{24}$$

$$\tilde{R}(2\bar{E}'\bar{R} + 2\bar{E}\bar{R}') + 2\bar{E}\bar{R}\tilde{R}' + \bar{R}(2\bar{R}'\tilde{E} + \bar{R}\tilde{E}') + \mathrm{Pe}[\tilde{R}(\bar{\sigma}'\bar{v} + \bar{\sigma}\bar{v}')$$
$$+ \tilde{\sigma}(\bar{R}'\bar{v} + \bar{v}'\bar{R}) + \tilde{v}(\bar{R}' + \bar{\sigma}) + \bar{v}(\bar{\sigma}\tilde{R}' + \bar{R}\tilde{\sigma}')] = -\mathrm{Pe}\,\omega(\bar{R}\tilde{\sigma} + \bar{\sigma}\tilde{R}), \tag{25}$$

$$\mathrm{Bi}\left(\frac{\bar{v}}{\bar{R}^2}\right)^{\frac{1}{3}}\left(1 + \frac{64V_{\mathrm{air}}^2}{\bar{v}^2}\right)^{-5/6}\left[\frac{10\tilde{R}(\bar{T} - T_\infty)}{3\bar{R}^2} - \frac{2(\bar{T} - T_\infty)\tilde{v}}{3\bar{R}\bar{v}} - \frac{128V_{\mathrm{air}}^2\tilde{T}}{\bar{R}\bar{v}^2} + \frac{640(\bar{T} - T_\infty)V_{\mathrm{air}}^2\tilde{R}}{3\bar{R}^2\bar{v}^2} - \frac{2\tilde{T}}{\bar{R}} \right]$$
$$- \mathrm{Pe}^T(\tilde{v}\bar{T}' + \bar{v}\tilde{T}' + \omega\tilde{T}) + 6\,\mathrm{Na}\exp[E_a(1/\bar{T} - 1)]\bar{v}'\tilde{v}' = 0. \tag{26}$$
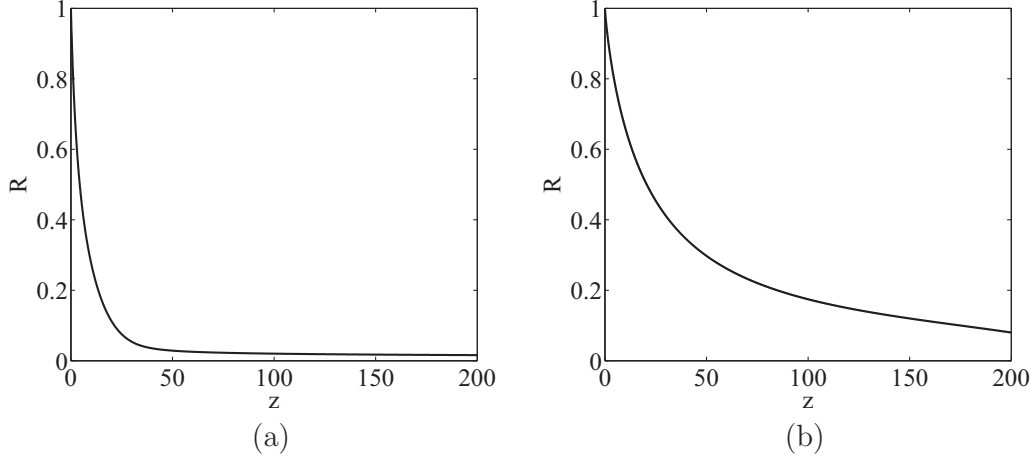
FIG. 3. Steady-state profile of dimensionless radius along the jet direction: (a) Set I; (b) Set II.

Here, $'$ represents differentiation with respect to z. The perturbation form of the boundary conditions to supplement the governing Eqs. (22)–(26) are

$$\text{At } z = 0: \quad \tilde{R}(0) = 0, \quad \tilde{v}(0) = 0, \quad \tilde{E}(0) = 0, \quad \tilde{\sigma}(0) = 0, \quad \tilde{T}(0) = 0. \tag{27}$$

$$\text{At } z = \chi: \quad 4\chi \tilde{R}' + \tilde{R} = 0, \quad \tilde{E}(\chi) = 0, \quad \text{for Set I fluid, and}$$
$$\chi \tilde{R}' + \tilde{R} = 0, \quad \tilde{E}(\chi) = 0, \qquad \text{for Set II fluid.} \tag{28}$$

The governing equations for the perturbation Eqs. (22)–(26) are numerically solved using the Chebyshev collocation technique. Here, the spatial domain $z = [0, \chi]$ is discretized in to N collocation points whose co-ordinates are given by the roots of the Chebyshev-Gauss-Lobatto polynomials. The discretized equations result in to a generalized eigenvalue problem of the form

$$M_A \tilde{\phi} = \omega M_B \tilde{\phi}, \tag{29}$$

where $\tilde{\phi}$ is an array of size $5N \times 1$, and M_A and M_B are the coefficient matrices of size $5N \times 5N$. Here, integer prefix 5 represents the number of jet variables, $\tilde{R}, \tilde{v}, \tilde{E}, \tilde{\sigma}$, and $\tilde{T}$ at each of the N collocation points. The eigenvalue problem is solved using numerical library package (DGEEV in LAPACK) to obtain a spectrum of complex eigenvalues ω, plotted in $\omega_r - \omega_i$ plane. By varying number of collocation points N, the spurious modes (nonoverlapping modes) are eliminated and physical eigenmode are identified. The modes with positive value of real part ω_r represent the axisymmetric instability modes, indicating unstable jet, leading to diametric oscillations and potential bead formation.

III. RESULTS AND DISCUSSION

A. Steady-state solution

The first step in performing linear stability analysis is to obtain the steady-state (the base-state) profile of the electrified jet. The dimensionless Eqs. (9)–(13) governing the jet dynamics are numerically solved under steady-state conditions using COMSOL Multiphysics 4.4. The steady-state profiles are obtained using the reference parameters for Set I and Set II fluids listed in Table I. Figure 2 plots the magnitude

of various forces acting on the jet along the z direction for Sets I and II fluids. In both the fluids, the surface tension and gravity force (not plotted) are weakest forces and have a little influence on the jet profile. For Set I which describes a low viscosity fluid with high electrical conductivity, the dominant forces are found to be the inertial and electric forces which counter-balance to give a steady jet profile. The viscous force affects the profile only close to the nozzle exit and becomes insignificant toward the end as jet thinning becomes weak. Thus, the force balance Eq. (17) has been confirmed by the numerical estimation of the forces. However, for Set II, which describes a highly viscous liquid with low electrical conductivity, the inertial force is very weak and the electrical force is balanced by the viscous force, as seen in Fig. 2(b). Thus, the force balance condition Eq. (19) adopted to derive the asymptotic condition at the lower end has been confirmed by the force profiles.

Figure 3 plots the steady-state radius of the thinning jet for the two reference fluids. For Set I fluid, the presence of a strong tangential electric force results into very strong thinning of jet radius, with a dramatic reduction in radius near the nozzle exit as shown in Fig. 3(a). However, for weakly conducting Set II fluid, the thinning is found to be moderate with a gradual reduction in radius as jet travels as shown in Fig. 3(b).

The difference in radius profiles of the two fluids can be explained with the help of profile depicting the distribution of surface charge density along the jet axis for the two cases as shown in Fig. 4. The surface charge density profile, $\sigma(z)$, for the highly conductive fluid (Set I) is shown in Fig. 4(a). At $z = 0$, the surface charge density is zero as charges reside in the bulk. Due to high electrical conductivity, the charges
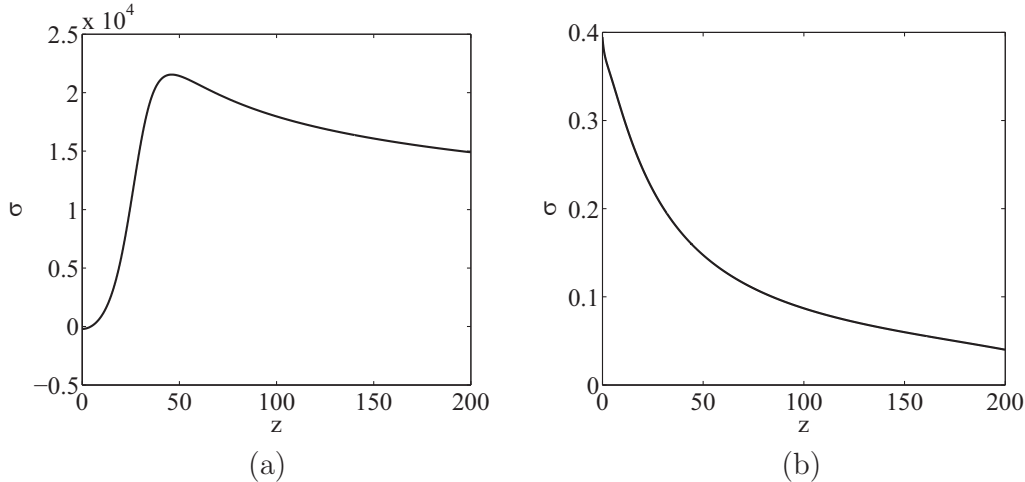
FIG. 4. Steady-state profile of dimensionless surface charge density along the jet axis: (a) Set I; (b) Set II.

migrate from bulk to the fluid-air interface leading to build up of surface charge density at short distance from the nozzle. The external electrical field acting on the surface charge build up generates strong electrical stresses which causes a substantial thinning of the jet indicated by a steep decrease in jet radius [refer to Fig. 3(a)]. Afterwards, as jet thins gradually, the surface charge density slowly drops due to charge repulsion. Fig. 4(b) plots the surface charge density profile, $\sigma(z)$, for the low conductivity fluid (Set II). Here, the peak value of surface charge density is orders of magnitude smaller compared to that for the high conductivity Set I fluid. The weakly conductive fluid is characterized by the absence of charge migration from bulk toward the surface and the axial charge distribution is primarily dominated by the charge convection as jet propagates. The smaller amount of surface charge density generates weak electrical stresses which in turn results in to weaker thinning of the jet producing thicker fibers. Moreover, the viscous forces hinder the fiber thinning, as inertia is smaller in magnitude, which also contributes to the formation of thicker fibers. Further, the gradual decrease in surface charge density correlates to the gradual thinning of the jet [refer to Fig. 3(b)]. The steady-state jet profiles, especially the surface charge density and electric field profiles, are qualitatively similar to the profiles reported in several earlier studies for Newtonian as well as polymeric fluids [8,9,11].

The role of heat transfer in fiber profile is examined next. The strength of convective heat transfer from fiber to the surrounding is given by Biot number Bi, the dimensionless heat transfer coefficient. Figure 5 shows effect of heat transfer on radius and temperature profiles of the jet for Set II parameters. The line for Bi = 0 (heat transfer coefficient being zero) represents the jet under nearly isothermal condition. A small increase in temperature is due to the viscous dissipation effect. Increasing convective heat transfer to the environment (increasing Bi) results in to drop in jet temperature. A small increase in Biot number leads to around 20% drop in jet temperature at the collector with respect to its value at the nozzle [31]. The enhancement in fluid viscosity due to cooling gives rise to thicker fibers. The terminal radius increases appreciable upon increasing the extent of heat transfer. The increase in

fiber radius on cooling is also observed for Set I fluid, though not shown for brevity.

The sensitivity of viscosity to temperature is parametrized by activation energy, E_a. Figure 6(a) illustrates the effect of activation energy on the jet radius profile for Set II fluid. The corresponding local value of fluid elongational viscosity (normalized by viscosity at nozzle temperature, η_0) along the jet, η_e/η_0 is depicted in Fig. 6(b). The thermal and inertial energy must be higher than the activation energy of material to allow translational motion of the molecules. Thus, higher activation energy, implying greater enhancement of viscosity for a given change in temperature, leads to a stronger increase in viscosity of the jet as it travels the straight path as shown in Fig. 6(b). The increase in viscosity for higher activation energy results in to thicker fibers as shown in Fig. 6(a).

B. Stability analysis

For linear stability analysis, the steady-state profile of thinning jet is treated as the base-state upon which nonperiodic axisymmetric disturbances are superimposed. The discrete set of growth rate of these disturbances is obtained as eigenvalues of the disturbance problem symbolically represented in Eq. (29). Numerical technique estimates a spectrum of the complex-valued growth rates $\omega = \omega_r + i\,\omega_i$ as eigenvalues and the corresponding $\tilde{\phi}(z)$ as eigenfunction. Figures 7 and 8 present the spectra of eigenvalues in ω_r-ω_i plane for the two reference fluids Set I and Set II, respectively. In both cases, eigenspectra are constructed for the isothermal condition (obtained by setting Bi = 0 and keeping other parameters unchanged) as well as the corresponding nonisothermal condition (Bi $\neq$ 0) in parts (a) and (b), respectively. To identify the physical eigenmodes and to eliminate the spurious modes, different numbers of collocation points N are considered. It is important to note only the leading mode, the one with the largest value of real part ω_r, is of interest and is dominant mode as it is the fastest growing (or slowest decaying) mode. As seen, the leading eigenvalue is fully converged upon varying the collocation points N.

For a high conductivity and low viscosity fluid (Set I), Fig. 7(a) shows that, for the isothermal conditions, a part of
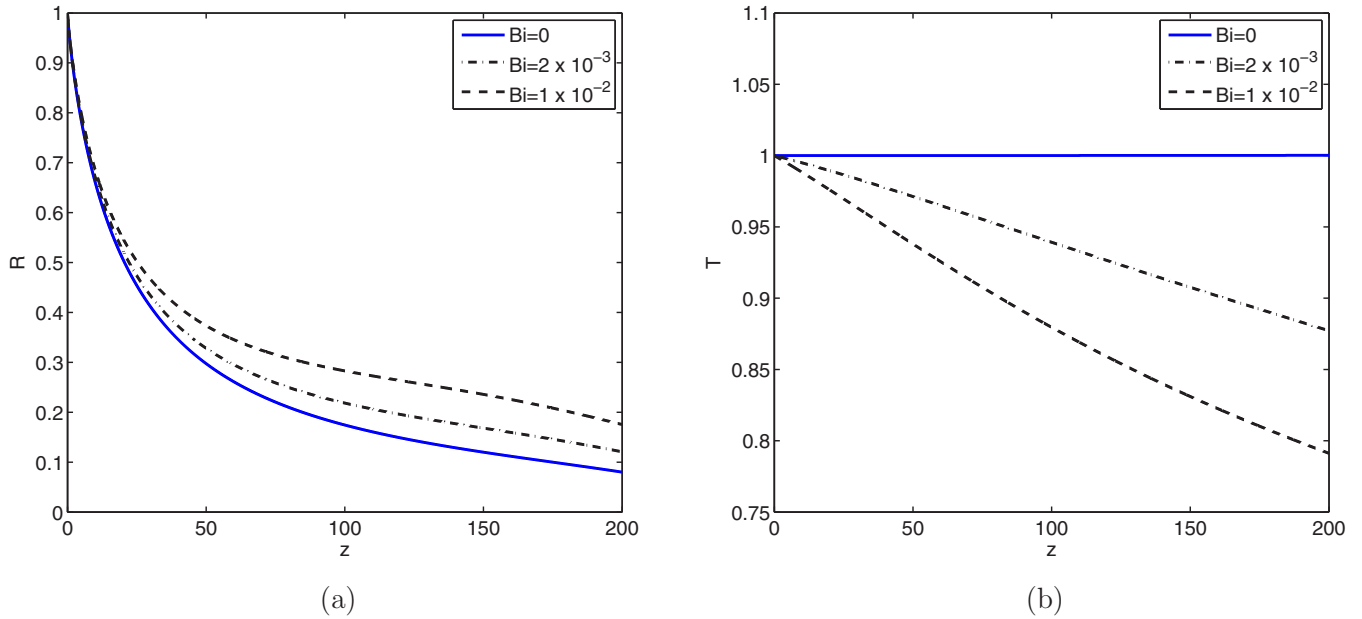
FIG. 5. Dimensionless steady-state profile of thinning jet for various Biot numbers: (a) radius; (b) temperature. Parameters: Set II.

the eigenspectrum lies on the positive side of ω_r. Therefore, the the leading growth rate is positive indicating an unstable jet. However, when the Biot number is made nonzero, keeping other parameters unchanged, the spectrum shifts toward the negative side of ω_r such that the maximum growth rate becomes negative. Thus, heat transfer renders the jet stable to axisymmetric disturbances. Similar stabilization of eigenmodes is also observed for the low conductivity and high viscosity fluid (Set II), as shown in Fig. 8. Hence, for both the reference fluids, while the isothermal jet is unstable, the nonisothermal jet is found to be stable under similar electrospinning conditions. The jet stabilization is attributed to modification in fluid viscosity upon cooling. The enhanced

viscous stresses tend to render the jet stable. Thus, the axisymmetric instability in the form of diametric oscillations can be suppressed and smooth fibers are obtained by inducing heat transfer from the jet.

In the present analysis, the only mechanism of heat transfer from the fiber to the surrounding air is convective heat transfer, as solvent evaporation is neglected. Convective heat transfer is controlled by two factors, the heat transfer coefficient h and the temperature difference $[T(z) - T_\infty]$. The heat transfer coefficient is characterized by the dimensionless Biot number. As heat transfer coefficient depends upon the local velocity of the jet v as well as the ambient air velocity V_{air}, the Biot number varies along the jet according to Eq. (14),
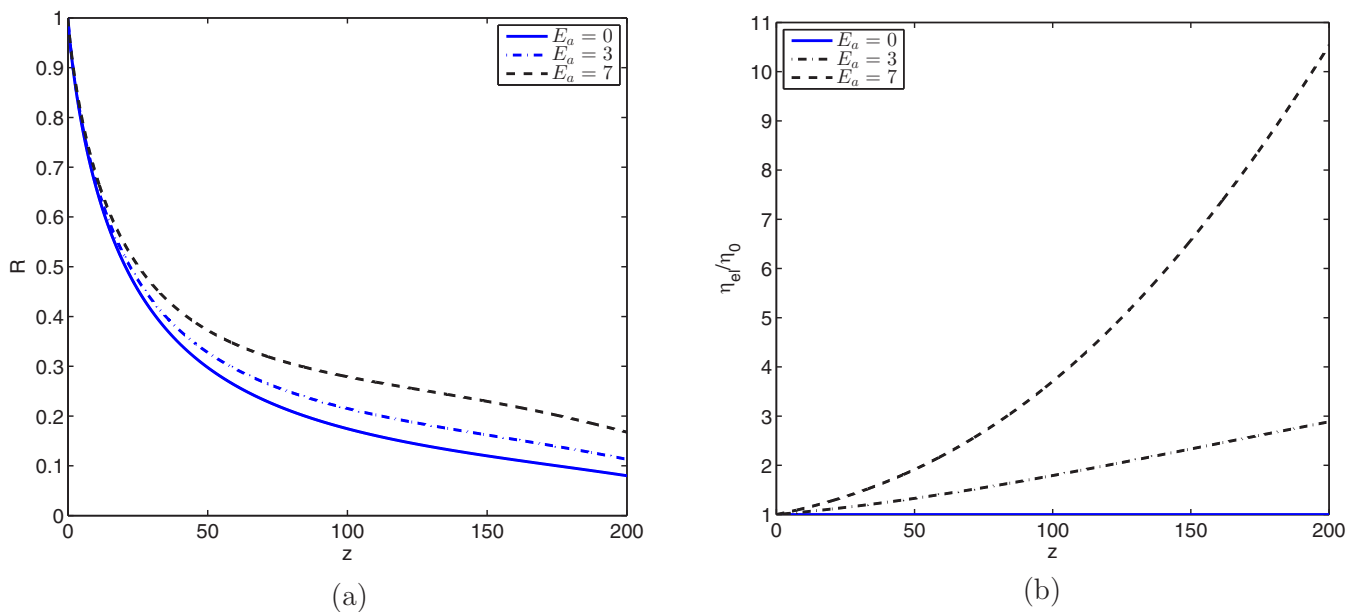

FIG. 6. Steady-state profile of thinning jet for different values of activation energies. (a) Dimensionless radius; (b) dimensionless elongational viscosity. Parameters: Set II.
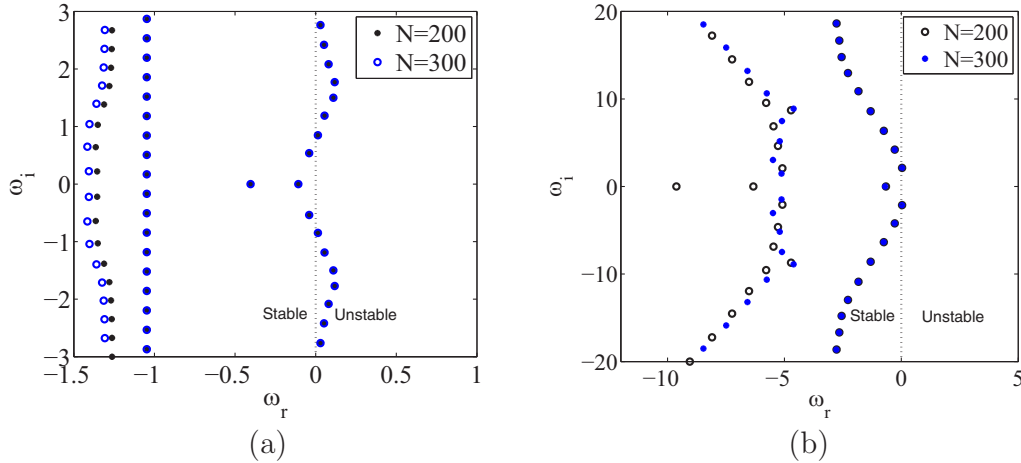
FIG. 7. Eigenspectrum for isothermal and nonisothermal jets: Real part of growth rate, ω_r, vs imaginary part of growth rate, ω_i, for a thinning jet with superimposed nonperiodic perturbations. (a) Bi $= 0.0$; (b) Bi $= 0.05$. Parameters: Set I.

where Bi is the Biot number at the nozzle ($z = 0$). The local Biot number Bi_z is found to be higher and increases as jet propagates and accelerates toward the bottom plate. Thus, heat transfer is much faster from the thinned jet (at high velocity) compared to the jet emanating from the nozzle (at relatively lower velocity). Figure 9 plots the variation in leading growth rate with Biot number, Bi (defined at the nozzle condition) for both the fluids. The leading growth rate is positive in the absence of heat transfer (Bi $= 0$) for both the fluids. Upon increasing heat transfer, the growth rate decreases and beyond a certain value of Biot number, it changes its sign from positive to negative. Thus, the axisymmetric instability can be suppressed by cooling of the jet. The temperature drop stabilizes the electrospun jet irrespective of the fluid conductivity. While for Set I fluid the stabilization role of cooling is observed for the entire range of Biot number examined, the stabilization effect of increasing Biot number appears to be arrested for the Set II fluid after the jet has stabilized. This may be due to a limit to which the viscous stresses developed upon cooling could stabilize the jet of fluid which is already highly viscous.

The effect of activation energy, which captures the degree of enhancement of viscosity upon cooling, on the the leading growth rate is shown in Fig. 10. For both types of fluids, the increase in activation energy tends to decrease the real part of the leading growth rate. For Set II fluid (high viscosity fluids), the stabilizing effect of activation energy is strong enough to shift the growth rate from unstable region ($\omega_r > 0$) to stable region ($\omega_r < 0$), as shown in Fig. 10(b). The fluid with higher activation energy generates greater viscous stresses upon cooling which are responsible for stabilization of the jet. As discussed earlier, the stabilization limit is attained for the high viscosity Set II fluid such that while growth rate decreases with initial increase in activation energy, it remains largely unchanged upon further increase in the value of activation energy.

The local heat transfer coefficient can be enhanced by subjecting the jet to a thermally cooled environment with a cross-current flow of surrounding gas, as described by Eq. (14). The air flow dramatically increases the local heat transfer coefficient throughout the jet, including near the nozzle where jet velocity is much lower. The jet velocity increases
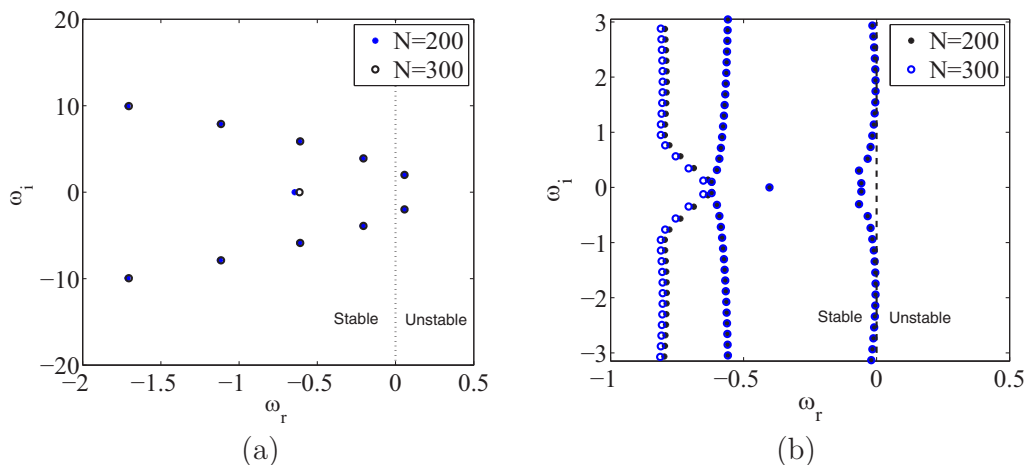

FIG. 8. Eigenspectrum for isothermal and nonisothermal cases: Real part of growth rate, ω_r, vs imaginary part of growth rate, ω_i, for a thinning jet with superimposed with nonperiodic perturbations. (a) Bi $= 0.0$; (b) Bi $= 0.07$. Parameters: Set II.
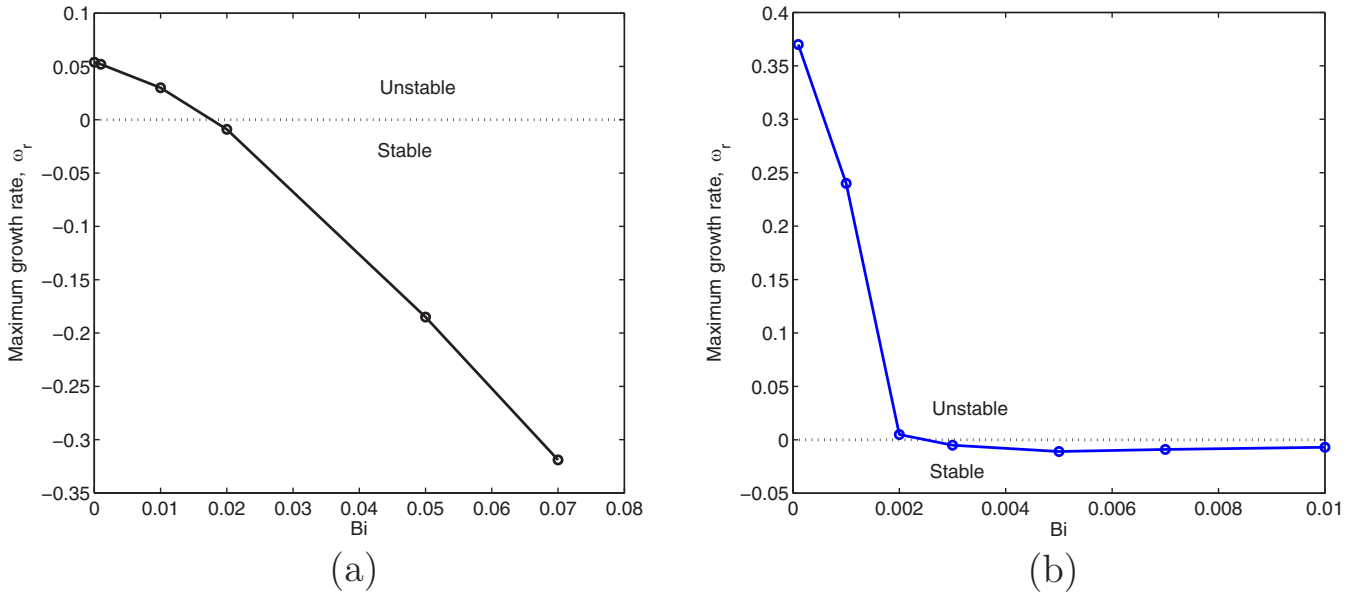
FIG. 9. Effect of heat transfer coefficient, Bi, on real part of the leading growth rate, ω_r, for thinning jet: (a) Set I; (b) Set II.

by an order of magnitude as the jet proceeds toward the collector. A lower end of the jet where $v \gg V_{air}$, effect of air velocity on the local Biot number becomes insignificant, as per Eq. (14). An overall increase in the local heat transfer coefficient owing to air flow is generally expected to affect the stability of the jet. Figure 11 plots the variation in the leading growth rate with air velocity for Set II fluid. The value of growth rate decreases marginally with increasing air velocity. The cooling effect of air flow, however, is not sufficient enough to entirely suppress the instability. The air flow increases the heat transfer coefficient only in the upper part of the jet, whereas the heat transfer in the middle and lower ends of the jet is entirely controlled by the jet momentum and is unaffected by the air velocity. Thus, the role of cooling

air flow in suppressing the axisymmetric instability of the electrified jet is found to be limited.

The above discussion presented the role of various parameters on the stability behavior. Next, we attempt to understand the mechanism of instability modes for both the reference fluids. Hohman *et al.* [4] suggested that there exits two types of axisymmetric instability modes in an electrified jet. The first one is the surface-tension-driven capillary mode, which is the classical Rayleigh-Plateau instability modified in the presence of an electric field. Here, the surface tension which tends to prevent jet breakup is a stabilizing force where as the axial electric field tends to overcome the effect of surface tension and provides a destabilizing effect. The leading growth rate for the capillary mode decreases upon increasing the
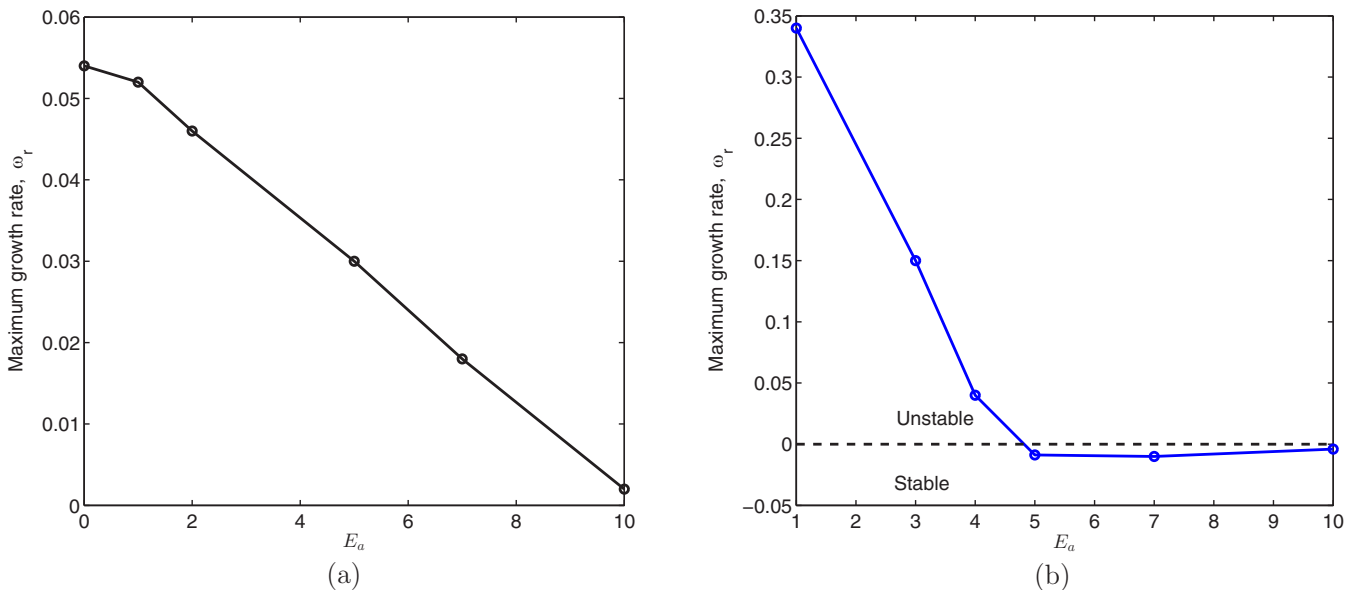

FIG. 10. Effect of activation energy on real part of the leading growth rate, ω_r, for thinning jet: (a) Set I; (b) Set II.
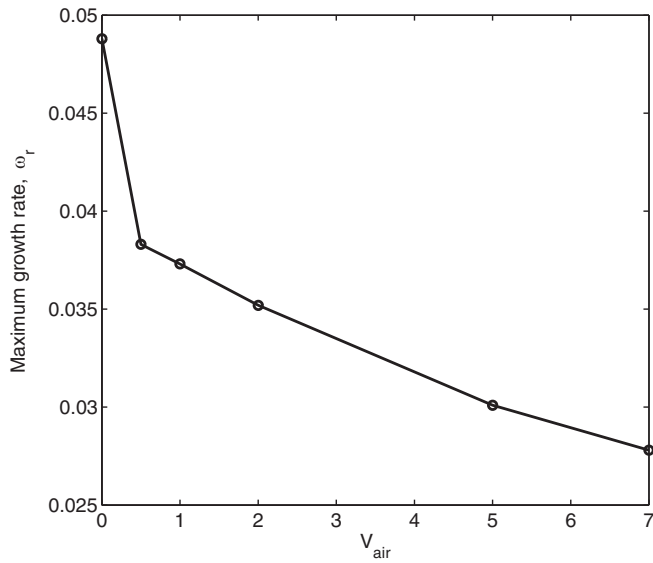
FIG. 11. Effect of air velocity, V_{air}, on real part of the leading growth rate, ω_r, for thinning jet. Parameters: Set II.

strength of external electric field strength. The second mode is the conducting mode of instability in which the instability is excited by the electric force generated by the coupling of surface charges and the electric field. Unlike capillary mode, the leading growth rate increases upon increasing the strength of external electric field for the conducting mode. As trend of leading growth rate upon varying electric field strength is opposite in both the modes, the electric field parameter can be used to identify the nature of instability mode for the two fluids being studied.

Figure 12 depicts the variation in leading growth rate with the strength of external electric field, E_∞ for both the fluids. For the high conductivity Set I fluid, increasing the electric field strength tends to increase the leading growth rate as shown in Fig. 12(a). For a strong enough electric field, the jet transitions from stable ($\omega_r < 0$) to unstable ($\omega_r > 0$) region. The destabilizing role of electric field implies that the dominant instability mode is conducting mode for Set I fluid
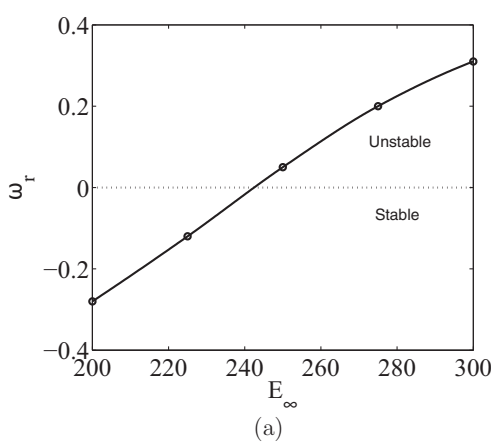
[4,13,14]. However, for highly viscous Set II fluid, increasing electric field tends to reduce the growth rate indicating stabilizing role. Hence, for a weakly conductive jet subjected to low electric field, the capillary mode dominates, whereas for a highly charged jet in a strong electric field, the instability is driven by the conducting mode [4]. Interestingly, both of these modes are stabilized by cooling of the jet.

Similar to electric field strength, the electrical conductivity of the fluid is another parameter that can distinguish between the two qualitatively different modes of instability. While capillary mode remains unaffected by electrical conductivity of the fluid, the conducting mode driven by the coupling of surface charges and electric field is primarily excited by the electrical conductivity of the fluid [4]. The effect of electrical conductivity on the leading growth rate ω_r is, therefore, examined next. The electrical conductivity, K, is captured by the dimensionless electric Péclet number. At the same, the conductivity also influences the dimensionless electric field at the nozzle, E_0, which in turn affects dimensionless field parameters, E_f and E_∞ (refer to Table I). Thus, varying K leads to simultaneous changes in Pe, E_f and E_∞ as per their dependence on conductivity, K. Figure 13 plots the variation in leading growth rate with electric Péclet number for both the sets. It should be noted that varying Péclet number captures variation in K and hence is accompanied by varying E_f and ∞ as per their definitions. Here, increasing electrical conductivity is represented by decreasing Péclet number. For Set I fluid, increasing conductivity (decreasing Pe) transitions the jet from stable to unstable region. Increasing electrical conductivity leads to a strong build up of surface charges which tends to destabilize the jet. The destabilizing role of electrical conductivity further confirms the nature of the leading mode for Set I fluid to be the conducting mode. This instability is qualitatively different from the classical Rayleigh-Plateau mode driven by the surface tension. For Set II fluid, as shown in Fig. 13(b), the variation in conductivity does not influence the leading growth rate significantly which confirms the instability mode to be the surface-tension-driven capillary mode.

Finally, the role of surface tension in stability behavior is examined by varying the capillary number. As shown in
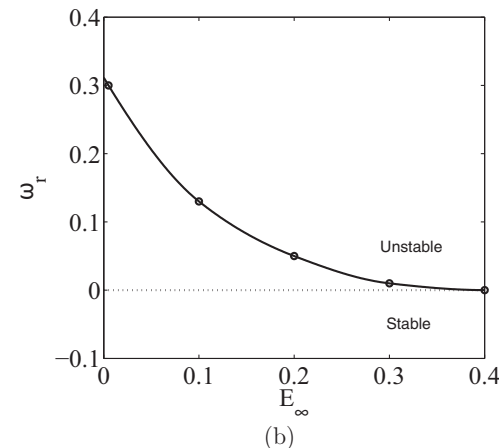

FIG. 12. Effect of external electric field, E_∞, on real part of the leading growth rate, ω_r, for thinning jet: (a) Set I: Conducting mode; (b) Set II: Capillary mode.
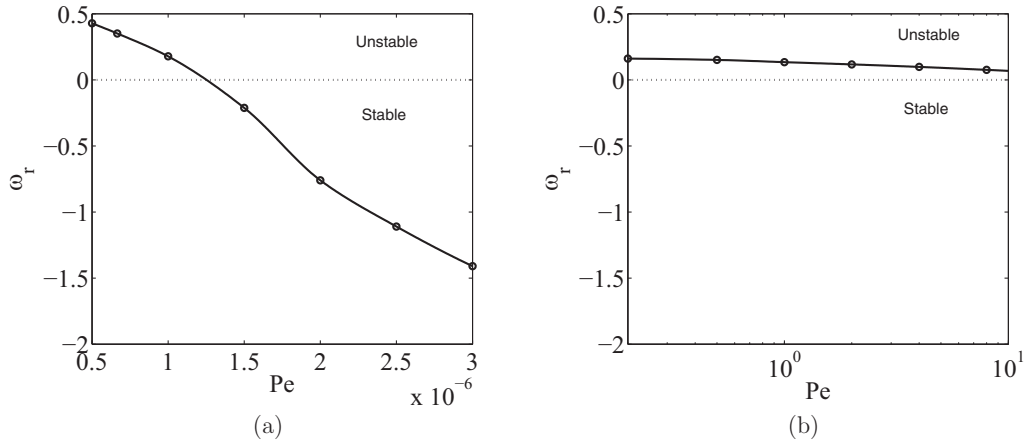
FIG. 13. Effect of conductivity given by electric Péclet number on real part of the leading growth rate, ω_r, for thinning jet: (a) Set I: Conducting mode; (b) Set II: Capillary mode.

Fig. 14, increasing surface tension (by decreasing capillary number) results in to increase in growth rate for both the reference fluids. The destabilizing effect of surface tension is more pronounced in Set II fluid for which the leading mode is the capillary mode.

An important feature of the present analysis is that the disturbances are imposed on a jet with thinning profile (with nonuniform distribution of jet variables). This is in contrast to most prior stability analyses in which the axisymmetric disturbances are imposed on a cylindrical jet of uniform radius and other jet variables [10–12]. The present analysis being more rigorous, therefore, accurately estimates the disturbance growth rate under realistic electrospinning conditions. It would be interesting to compare the growth rate for a thinning jet with that obtained by assuming uniform jet as the base-state. For the later case, the uniform jet variables, including radius, are taken as their terminal values, *i.e.* at the lower end of the jet. Figure 15 compares the leading growth rate values for two different base-states, the thinning jet and the uniform radius jet. The comparisons are plotted for both the reference fluid under varying heat transfer conditions. For

both sets, the growth rate is found to be smaller in magnitude for the thinning jet as compared to the uniform jet. Importantly, for Set I fluid, the growth rate for thinning jet is found to be an order of magnitude smaller than that for the uniform jet. The differences are not just in magnitude but also the sign of growth rate, thus altering the key conclusion of the stability analysis. At large Biot number, while the cylindrical jet of radius equal to the terminal radius of the thinned jet is predicted to be unstable, the more rigorous analysis of thinning jet profile finds the jet to be stable. The reduction in the real part of the growth rate of the thinning jet results from inclusion of the deformation strain in thinning base-state profile of the electrified jet. The simplified uniform cylinder profile disregards the gradients of all jet variables, most importantly the velocity gradient responsible for the stabilizing viscous forces is ignored. Moreover, the nonuniform distribution of surface charge density as well as axial electric field, ignored in the uniform jet analysis, play an important role in the stability behavior. Thus, the entire profile of the thinning jet is essential in accurate estimation of the disturbance eigenspectrum. It should, however, be noted that for both the analyses of
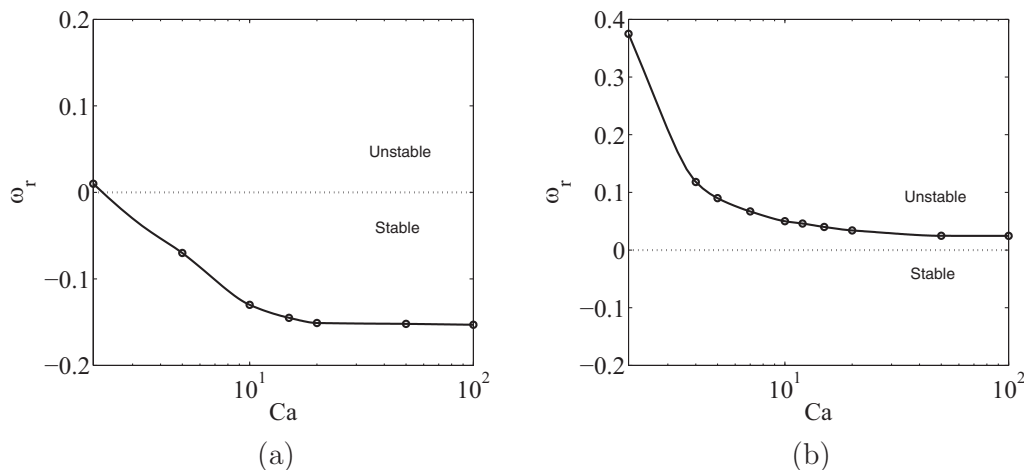

FIG. 14. Effect of capillary number, Ca, on real part of the leading growth rate, ω_r, for thinning jet: (a) Set I: Conducting mode; (b) Set II: Capillary mode.
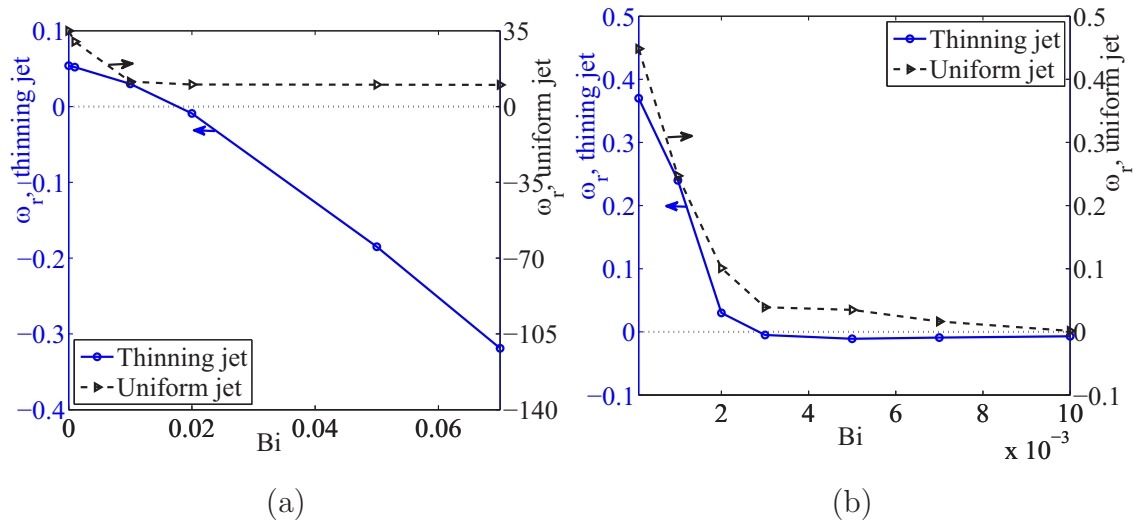
FIG. 15. Maximum growth rate of disturbance corresponding to thinning jet and uniform jet. Parameters for various heat transfer coefficients, Bi: (a) Set I; (b) Set II.

thinning jet and uniform radius jet, the role of heat transfer is found to be stabilizing as leading growth rate decreases upon increasing the Biot number.

In the electrospinning process, the nonsmooth beaded fibers are produced in a certain range of operating and material parameters. The present analysis provides useful means to optimize the electrospinning parameters such that the undesirable axisymmetric instability is suppressed and defect-free smooth fibers are produced. Finally, it is important to note that while solvent evaporation is ignored in the present analysis, the recent study examines the role of solvent evaporation in stability of an electrified jet [36]. For electrospinning of polymeric solutions, the evaporation of solvent during the straight jet path tends to weaken or completely suppress the axisymmetric instability. The stabilization attributed to the enhancement in fluid viscosity and elasticity upon solvent removal results in to production of smooth fibers without bead formation.

IV. CONCLUSION

An electrified jet of Newtonian fluid under nonisothermal condition is analyzed to estimate the onset of an axisymmetric instability which manifests in the form of growing oscillations in fiber diameter. The study addresses the conditions leading to the formation of electrospun nanofibers with thick-thin variations, a precursor for beaded fibers. The eigenspectrum of growth rates of axisymmetric disturbances is constructed using the linear stability theory. Unlike most prior studies which treat the jet as uniform radius cylinder, the present analysis examines the stability behavior of a jet with *thinning* profile under the action of tangential electric field. The study is relevant to high-temperature electrospinning of weakly elastic materials (either melt or solutions), treated as Newtonian

fluids. The role of convective heat transfer from fiber to the ambient air, in the absence of any mass transfer, in stability behavior is examined.

The enhancement in fluid viscosity, due to transfer of thermal energy from fiber to the surrounding, results in to thicker fibers. The stability analysis reveals that the conducting mode of instability is dominant for high conductivity (and low viscosity) fluid. In this case, increase in magnitude of imposed electric field and fluid conductivity tend to increase the growth rate of leading disturbance suggesting destabilizing role of tangential electric stress, indicating conducting mode of instability. However, for the low conductivity (and high viscosity) fluid, the stabilizing role of electric field is observed. Thus, in this case, the leading mode is classical Rayleigh-Plateau mode driven by surface tension which is known to be stabilized by tangential electric field. For both fluids, the heat transfer from fiber to the surrounding is found to stabilize the axisymmetric instability. The growth rate decreases upon heat transfer and it changes its sign from positive (unstable jet) to negative (stable jet) for certain high enough heat transfer coefficient. The stabilizing role of heat transfer is attributed mainly to the increase in fluid viscosity upon cooling leading to enhanced magnitude of stabilizing viscous stresses. Thus, the axisymmetric instability potentially leading to undesirable bead formation along the fiber can be entirely suppressed by inducing heat transfer from the fiber.

Further, it is observed that the thinning jet is relatively more stable compared to cylindrical jet of uniform radius. The analysis, thus, more accurately estimates the stability behavior of a jet experiencing thinning as well as nonuniform distribution of surface charge density and axial electric field under realistic electrospinning conditions. The analysis offers guidelines for designing a nonisothermal electrospinning process to produce smooth bead-free fibers.

[1] L. H. Zhang, X. P. Duan, X. Yan, M. Yu, X. Ning, Y. Zhao, and Y. Z. Long, Recent advances in melt electrospinning, RSC Adv. **6**, 53400 (2016).

[2] K. Garg and G. L. Bowlin, Electrospinning jets and nanofibrous structures, Biomicrofluidics **5**, 013403 (2011).

[3] T. D. Brown, P. D. Dalton, and D. W. Hutmacher, Melt electrospinning today: An opportune time for an emerging polymer process, Prog. Polym. Sci. **56**, 116 (2016).

[4] M. M. Hohman, M. Shin, G. Rutledge, and M. P. Brenner, Electrospinning and electrically forced jets I: Stability theory, Phys. Fluids **13**, 2201 (2001).

[5] F. Li, A. M. Gãńan Calvo, and J. M. López-Herrera, Absolute-convective instability transition of low permittivity, low conductivity charged viscous liquid jets under axial electric fields, Phys. Fluids **23**, 094108 (2011).

[6] A. M. Gãńan Calvo, Cone-Jet Analytical Extension of Taylor's Electrostatic Solution and the Asymptotic Universal Scaling Laws in Electrospraying, Phys. Rev. Lett. **79**, 217 (1997).

[7] J. R. Melcher and G. I. Taylor, Electrohydrodynamics: A review of the role of interfacial shear stresses, Annu. Rev. Fluid Mech. **1**, 111 (1969).

[8] J. J. Feng, The stretching of an electrified non-Newtonian jet: A model for electrospinning, Phys. Fluids **14**, 3912 (2002).

[9] J. J. Feng, Stretching of a straight electrically charged viscoelastic jet, J. Non-Newtonian Fluid Mech. **116**, 55 (2003).

[10] C. P. Carroll and Y. L. Joo, Electrospinning of viscoelastic Boger fluids: Modeling and experiments, Phys. Fluids **18**, 053102 (2006).

[11] C. P. Carroll and Y. L. Joo, Axisymmetric instabilities of electrically driven viscoelastic jets, J. Non-Newtonian Fluid Mech. **153**, 130 (2008).

[12] C. P. Carroll and Y. L. Joo, Axisymmetric instabilities in electrospinning of highly conducting, viscoelastic polymer solutions, Phys. Fluids **21**, 103101 (2009).

[13] J. M. Deitzel, J. Kleinmeyer, D. Harris, and N. C. B. Tan, The effect of processing variables on the morphology of electrospun nanofibers and textiles, Polymer **42**, 261 (2001).

[14] M. M. Demir, I. Yiglor, E. Yiglor, and B. Erman, Electrospinning of polyurethane fibers, Polymer **43**, 3303 (2002).

[15] J. M. Lopez-Herrera, A. M. Gãńan Calvo, and M. Perez-Saborid, One-dimensional simulation of the breakup of capillary jets of conducting liquids. Application to E. H. D. spraying, J. Aerosol Sci. **30**, 895 (1999).

[16] J. M. López-Herrera and A. M. Gãńan Calvo, A note on charged capillary jet breakup of conducting liquids: experimental validation of a viscous one-dimensional model, J. Fluid Mech. **501**, 303 (2004).

[17] J. M. López-Herrera, P. R. Chueca, and A. M. Gãńan Calvo, Linear stability analysis of axisymmetric perturbation in imperfectly conducting liquid jets, Phys. Fluids **17**, 034106 (2005).

[18] C. Wang, Y. W. Cheng, C. H. Hsu, H. S. Chien, and S. Y. Tsou, How to manipulate the eletrospinning jet with controlled properties to obtain uniform fibers with the smallest diameter A brief discussion of solution electrospinning process, J. Polym. Res. **18**, 111 (2011).

[19] F. Li, X. Y. Yin, and X. Z. Yin, Absolute and convective instability of a coaxial viscous liquid jet under both axial and radial electric fields, E. J. Mech. B/Fluids **55**, 39 (2016).

[20] F. Li, X. Y. Yin, and X. Z. Yin, Transition from a beads-on-string to a spilke structure in an electrified viscoelastic jet, Phys. Fluids **29**, 023106 (2017).

[21] Q. Wang, S. Mahalmann, and D. T. Papageorgiou, Dynamics of liquid jets and threads under the action of radial electric fields: microthread formation and touchdown singularities, Phys. Fluids **21**, 032109 (2009).

[22] Dharmansh and P. Chokshi, Axisymmetric instability in a thinning electrified jet, Phys. Rev. E **93**, 043124 (2016).

[23] D. Deshawar and P. Chokshi, Stability analysis of a thinning polymeric electrified jet, Polymer **131**, 34 (2017).

[24] K. Gupta and P. Chokshi, Weakly nonlinear stability analysis of polymer fibre spinning, J. Fluid Mech. **776**, 268 (2015).

[25] K. Gupta, P. Chokshi, and R. Stepanyan, Die-swell effect in draw resonance of polymeric spin-line, J. Non-Newtonian Fluid Mech. **230**, 1 (2016).

[26] K. Gupta and P. Chokshi, Stability analysis of bilayer polymer fiber spinning process, Chem. Eng. Sci. **174**, 277 (2017).

[27] K. Gupta and P. Chokshi, Stability analysis of nonisothermal fibre spinning of polymeric solutions, J. Fluid Mech. **851**, 573 (2018).

[28] L. Larrondo and R. St. J. Manley, Electrostatic fiber spinning from polymer melts. I. Experimental observations on fiber formation and properties, J. Polym. Sci. Polym. Phys. Ed. **19**, 909 (1981).

[29] J. S. Kim and D. S. Lee, Thermal properties of electrospun polyesters, Polym. J. **32**, 616 (2000).

[30] J. Lyons, C. Li, and F. Ko, Melt-electrospinning. Part I: Processing parameters and geometric properties, Polymer **45**, 7597 (2004).

[31] E. Zhmayev, H. Zhou, and Y. L. Joo, Modeling of nonisothermal polymer jets in melt electrospinning, J. Non-Newtonian Fluid Mech. **153**, 95 (2008).

[32] E. Zhmayev, D. Cho, and Y. L. Joo, Nanofibers from gas-assisted polymer melt electrospinning, Polymer **51**, 4140 (2010).

[33] A. Karchin, F. I. Simonovsky, B. D. Ratner, and J. E. Sanders, Melt electrospinning of biodegradable polyurethane scaffolds via melt spinning and electrospinning, Acta Biomater. **7**, 3277 (2011).

[34] H. J. Zhou, T. B. Green, and Y. L. Joo, The thermal effects on electrospinning of polylactic acid melts, Polymer **47**, 7497 (2006).

[35] D. Deshawar and P. Chokshi, Analysis of axisymmetric instability in polymer melt electrospinning jet, J. Non-Newtonian Fluid Mech. **255**, 1 (2018).

[36] D. Deshawar, K. Gupta, and P. Chokshi, Electrospinning of polymer solutions: An analysis of instability in a thinning jet with solvent evaporation, Polymer **202**, 122656 (2020).

[37] D. A. Saville, Stability of electrically charged viscous cylinders, Phys. Fluids **14**, 1095 (1971).

[38] Y. I. Frenkel, *Kinetic Theory of Liquids* (Dover, New York, 1955).

[39] T. Matsuo and S. Kase, Studies on melt spinning. VII. Temperature profile within the filament, J. Appl. Polym. Sci. **20**, 367 (1976).

[40] V. N. Kirichenko, I. V. Petryanov-Sokolov, N. N. Suprun, and A. A. Shutov, Asymptotic radius of a slightly conducting liquid jet in an electric field, Sov. Phys. Dokl. **31**, 611 (1986).